C Journal of Carbon Research

MDPI

Article

Electrochemical Li Storage Properties of Carbon-Rich B–C–N Ceramics

Shrikant Bhat [1], Pradeep Vallachira Warriam Sasikumar [1], Leopoldo Molina-Luna [2], Magdalena Joanna Graczyk-Zajac [1,*], Hans-Joachim Kleebe [2] and Ralf Riedel [1]

[1] Institut für Materialwissenschaft, Technische Universität Darmstadt, 64289 Darmstadt, Germany; bhat@materials.tu-darmstadt.de (S.B.); pradeep@materials.tu-darmstadt.de (P.V.W.S.); riedel@materials.tu-darmstadt.de (R.R.)

[2] Institut für Angewandte Geowissenschaften, Technische Universität Darmstadt, 64289 Darmstadt, Germany; molina@geo.tu-darmstadt.de (L.M.-L.); kleebe@geo.tu-darmstadt.de (H.-J.K.)

* Correspondence: graczyk@materials.tu-darmstadt.de; Tel.: +49-061-5116-6343

Academic Editor: I. Francis Cheng
Received: 15 January 2016; Accepted: 18 March 2016; Published: 24 March 2016

Abstract: Amorphous BCN ceramics were synthesized via a thermal conversion procedure of piperazine–borane and pyridine–borane. The synthesized BC_2N and BC_4N ceramics contained, in their final amorphous structure, 45 and 65 wt % of carbon, respectively. Elemental analysis revealed 45 and 65 wt % of carbon for BC_2N and BC_4N, respectively. Transmission electron microscopy (TEM) and X-ray diffraction (XRD) confirmed the amorphous nature of studied compounds. Lateral cluster size of carbon crystallites of 7.43 and 10.3 nm for BC_2N and BC_4N, respectively, was calculated from Raman spectroscopy data. This signified a higher order of the carbon phase present in BC_4N. The electrochemical investigation of the low carbon BC_2N composition as anodes for Li-ion batteries revealed initial capacities of 667 and 235 mAh$\cdot$ g^{-1} for lithium insertion/extraction, respectively. The material with higher carbon content, BC_4N, disclosed better reversible lithium storage properties. Initial capacities of 1030 and 737 mAh$\cdot$ g^{-1} for lithium insertion and extraction were recovered for carbon-rich BC_4N composition. Extended cycling with high currents up to 2 C/2 D revealed the cycling stability of BC_4N electrodes. Cycling for more than 75 cycles at constant current rates showed a stable electrochemical behavior of BC_4N anodes with capacities as high as 500 mAh$\cdot$ g^{-1}.

Keywords: BCN ceramics; Li-ion batteries; rate capability; cycling stability

1. Introduction

Rechargeable lithium ion batteries are currently dominating the field of portable electronics. Considerable attention has been devoted to improving the performance of various insertion materials to meet the requirements of new technologies. Conventional anode materials for Li-ion batteries are based on graphite, which has a theoretical Li storage capacity of 372 mAh$\cdot$ g^{-1} with the formation of an intercalation compound LiC_6. Different forms of carbon-based materials with improved capacities and cycling performances have been widely investigated as an alternative to graphitic anodes [1–5]. Systems that react with lithium via conversion (e.g., Fe_2O_3 and SnO_2) or alloying (e.g., Si, Sn, and Al) mechanisms [6–12] deliver much higher capacities than graphite. However, the major drawback related to these materials is their poor cycling stability, which emerges from large volume expansion and contraction during Li-uptake and release.

Polymer-derived ceramic (PDC) anodes with *in-situ* generated disordered carbons embedded in an amorphous ceramic matrix are potentially promising candidates to be used as electrode materials. Within recent years, anode materials based on carbon-rich SiOC and SiCN PDCs have been widely investigated for their lithium storage properties [13–28]. It has been reported that carbon-rich

silicon carbonitride (SiCN) recovers capacities as high as 600 mAh· g^{-1}[25] while storing lithium mostly in the carbon phase [23,28]. The composite materials consisting of graphite/carbon-poor SiCN or precursor-derived Si(B)CN coated-multiwalled carbon nanotube (CNT) composite exceed by far the sum of the capacities of the single components [27,29,30]. Further, promising efforts have been done by using SiCN as stabilizing matrix for MoS_2 [31] and boron nitride [32]. Core-shell silicon oxycarbide—carbon nanotubes composites demonstrate extremely high capacities of ~800 mAh· g^{-1} and good capacity recovering at high current [33], while embedding of silicon nanoparticles in SiOC matrix lead to material stabilization with respect to prolonged cycling [34,35]. Outstanding electrochemical properties of SiOC and SiCN materials with respect to reversible lithium storage have been explained in relation to their complex amorphous nanostructure and the presence of a high amount of disordered free carbon distributed in the final ceramic matrix [28,36–38]. However, initial irreversible capacity loss is still a concern for these silicon-based PDCs.

Few reports provide information on the ion reversible hosting properties of carbon-based layered electrodes having other light atoms such as boron and nitrogen distributed within the carbon network. Nevertheless, heteroatom substitution in carbonaceous material is found to improve the electrochemical performance towards lithium storage. Doping with nitrogen or boron is an interesting approach to enhancing the performance of carbon-based anodes [39–42]. Boron-doped carbon has been reported to improve reversible Li storage capacity compared to pristine materials [43]. Boron or nitrogen-doped graphene have been investigated with respect to its use as an electrode in Li-ion batteries and demonstrated excellent capacities in the range of 1000 mAh· g^{-1} and stability with respect to very high currents charge/discharge [44]. Nevertheless, likely due to their particular morphology and microstructure, these materials suffer from substantial irreversible first insertion losses of around 50%, poor extended cycling efficiency of 95%–96%, and significant hysteresis.

Concerning B–C–N systems, only a handful of materials have been investigated with respect to the lithium storage properties. Ishikawa *et al.* [40] was the first to explore BCxN, systems (x = ~3, 7, 19) as anode materials, and found that storage capacity increases with an increase in the carbon content. The observed capacities were in the range of 180 mAh· g^{-1} for the studied materials. Later, Kawaguchi *et al.* [45] studied graphitic BC_6N materials for anode materials. BC_6N had an improved capacity of 303 mAh· g^{-1} during first discharge. These studies showed that Li-intercalation into bulk BCNs occurred with a smaller interlayer expansion ratio than that of graphite, thus suggesting better cyclability. However, these bulk materials exhibited low capacity. Recently, Lei *et al.* [39] reported nanostructured B–C–N layers with improved capacities of 390 mAh· g^{-1} and cycling stabilities at higher current rates.

For the present work, B–C–N ceramics were synthesized from amine boranes (piperazine–borane and pyridine–borane) through a high-temperature pyrolysis process. Two different compositions of polymer-derived BCN systems, namely, BC_2N and BC_4N, were investigated for lithium storage properties. Both compositions have revealed good cyclability; in particular, carbon-rich BC_4N ceramics showed reversible Li storage capacity as high as 735 mAh· g^{-1} at a slow rate.

2. Results and Discussion

The results of elemental analysis of C, N, and O content in the final BC_2N and BC_4N ceramics are listed in Table 1. Both samples are homogeneous with less standard deviation (5 random samples average data presented). The C to N ratio of 1.85 and 3.97 confirms the empirical formula BC_2N and BC_4N. The minor amount of oxygen of 2.4 and 1 wt % analyzed in BC_2N and BC_4N, respectively, is due to the manipulation of the samples in air. The amount of carbon in the final ceramics equals 45 wt % for BC_2N and 65 wt % for BC_4N.

Table 1. Bulk elemental analysis results of the synthesized BCN ceramics.

C [wt %]	N [wt %]	O [wt %]	Empirical Formula
45.7 ± 0.9	29.17 ± 1.8	2.41 ± 0.2	$BC_{1.85}N_{1.01}O_{0.08}$ ~ BC_2N
65.5 ± 1.3	18.32 ± 1.7	0.95 ± 0.25	$BC_{3.97}N_{0.95}O_{0.04}$ ~ BC_4N

XRD patterns of the precursors are shown in Figure 1, indicating the amorphous nature of both BC_2N and BC_4N compositions. The broad reflections observed in the diffraction patterns (marked with *) are due to the turbostratic nature of the BCN [46,47].

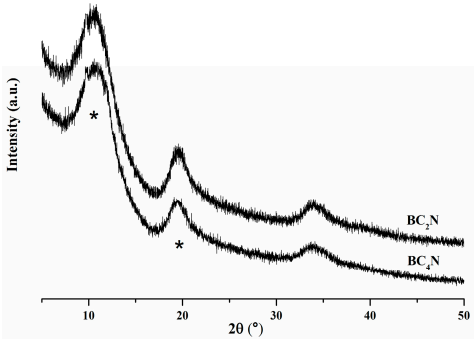

Figure 1. XRD patterns for synthesized BC_2N and BC_4N. Reflexes * stem from turbostratic nature of BCN [46,47].

The results of XPS measurements of the BC_2N and BC_4N have been reported in a previous study [48]. It confirms the presence of C–C, C–N, N–C, N–B, B–N and B–N–C [49,50] bonds and indicates the presence of C–O or C=O bonds in BC2N due to the surface oxygen (2.4%), as already revealed by elemental analysis. The presence of a noticeable amount of N–C, C–N [51], and B–N–C [49] bonds is also unambiguous. Raman spectra for both amorphous BC_2N and BC_4N compounds are presented in Figure 2. In both spectra, D (1350 cm^{-1}) and G (1580 cm^{-1}) bands are present, characteristic of carbonaceous materials. The presence of the intense D band approves the amorphous nature of the carbon phase, well corresponding to the absence of any graphite diffraction intensity in the XRD patterns. The well-pronounced G band is attributed to the presence of an ideal graphitic lattice vibration mode with E_{2g} symmetry. These findings are also consistent with the earlier report on amorphous BC_2N [52]. One can easily notice that G band contribution is more prominent in amorphous BC_4N compounds. The lateral cluster size (La) values is calculated by using the following equation proposed by Cancado *et al.* [53] with a laser wavelength of λ = 488 nm. In order to determine the integral (area) intensities of the D-band (I_D) and G-band (I_G), the 2-peaks (D and G) fitting using the Breit–Wigner–Fano (BWF) function was applied [54].

$$L_a\,(nm) = \left(2.4\ \times\ 10^{-10}\right) \times \lambda^4 \times \left(\frac{I_D}{I_G}\right)^{-1}$$

The L_a values for amorphous BC_2N and BC_4N compounds are found to be around 7.43 and 10.3 nm respectively. These results confirm that the carbon phase within amorphous BC_4N compounds demonstrates a more ordered nature compared to the free carbon phase within amorphous BC_2N.

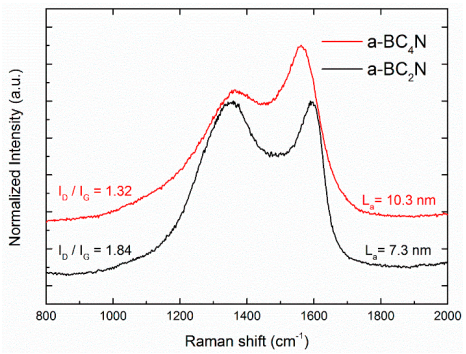

Figure 2. Raman spectra of BCN ceramics.

TEM micrographs for both BC_2N and BC_4N are presented in Figure 3. The corresponding selected area electron diffraction (SAED) image and EDX spectrum are shown in the inset. The SAED and TEM images confirm the amorphous nature of investigated materials. The TEM EDX analysis of different regions of the sample indicates the homogeneity (well dispersed B, C, and N). The intensity ratios analysis of the B, C, and N peaks in the EDX spectrum consistently showed the BC_2N and BC_4N composition for the respective sample. Oxygen contamination is also confirmed.

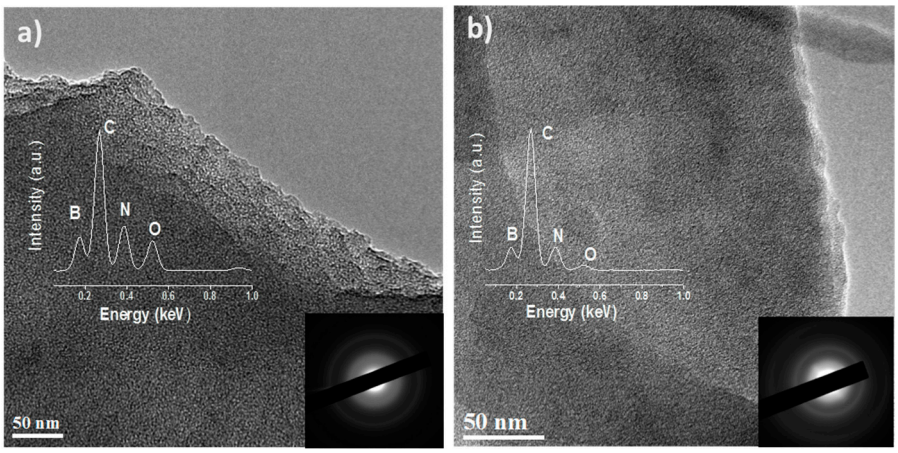

Figure 3. TEM images of the BC_2N (**a**) and BC_4N (**b**) ceramics. The corresponding selected area electron diffraction (SAED) image and EDX spectrum are shown in the inset.

The first cycle charge/discharge profiles of BC_2N and BC_4N electrodes are presented in Figure 4. The charging/discharging rate is the same both for lithium insertion and extraction, equal to 18 mA$\cdot g^{-1}$; the data are summarized in Table 2. The charging and discharging capacities of the BC_2N amount to 667 and 235 mAh$\cdot g^{-1}$, respectively. The BC_2N material reveals a large irreversible capacity loss during the first cycle, with a columbic efficiency of around 30%. Columbic efficiency η is obtained by a simple correlation of the first cycle insertion capacity (C_{ins1st}) and first cycle extraction capacity ($C_{extr1st}$), $\eta = C_{extr1st}/C_{ins1st} \times 100\%$. The first cycle charging capacity of BC_4N is much higher and amounts to 1030 mAh$\cdot g^{-1}$, while the discharge capacity amounts to 737 mAh$\cdot g^{-1}$, with a much higher first cycle efficiency of 72%. It should also be noted that most of the capacity is recovered below 1.5 V, and the investigated materials present reduced hysteresis in comparison to other polymer-derived electrode material [18,36].

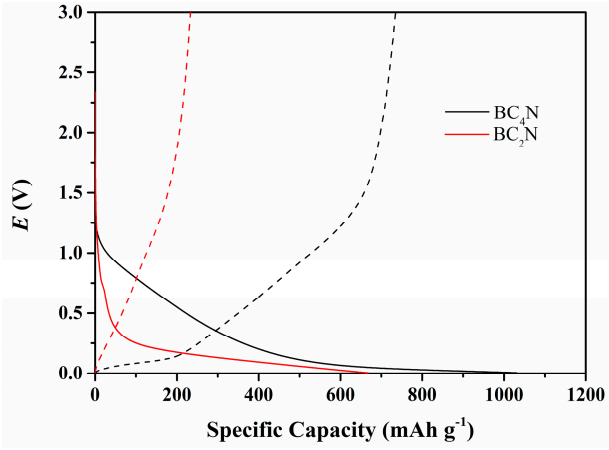

Figure 4. First cycle lithiation/delithiation profiles of studied BCN samples at a rate of C/20 (18 mA$\cdot g^{-1}$); solid line represents lithiation, and dotted line represents delithiation.

Table 2. Electrochemical capacity data for BC_2N and BC_4N ceramics.

Sample	Capacity $Li_{insertion}$ (mAh· g^{-1})	Capacity $Li_{extraction}$ (mAh· g^{-1})	Efficiency η (%)	Capacity Recovery (mAh· g^{-1})
BC_2N	667	235	35	265
BC_4N	1030	737	72	600

The capacities of the BC_2N and BC_4N recovered during extended cycling with an increasing rate are presented in Figure 5. Initially at slow rates, the fading of the capacity is registered. The values stabilize after 10–15 cycles and remain stable during extended cycling periods. BC_2N cells show good cycling stability but low capacities of 125 mAh· g^{-1} at C/2 rate, ~100 mAh· g^{-1} at C rate, and ~80 mAh· g^{-1} at 2 C rate. BC_4N gains the stability after 15 cycles and recovers capacities of ~400 mAh· g^{-1} at C/2 (180 mA· g^{-1}), ~300 mAh· g^{-1} at C (360 mA· g^{-1}), and ~200 mAh· g^{-1} is maintained at a rate of 2 C (720 mA· g^{-1}).

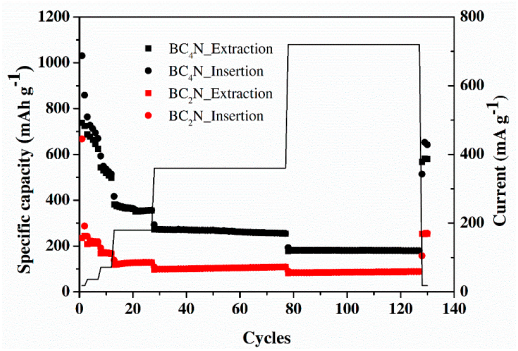

Figure 5. Electrochemical cycling of BCN samples at different current rates, from C/20 to 2 C (18 mA· g^{-1}–720 mA· g^{-1}).

Both BCN compounds demonstrate good capacity recovery when the initial rate imposed after high currents. A reversible capacity of 600 mAh g^{-1} is recovered for BC_4N cells, and a capacity of ~265 mAh· g^{-1} is recovered in case of the BC_2N electrode, respectively.

The BC_4N cells with high specific capacity were subjected to cycling at a constant rate of 75 cycles at 100 mA· g^{-1} to determine the long term cycling stability. The cycling data is presented in Figure 6. The cells cycled at this rate have an initial charging capacity of 730 mAh· g^{-1} and a discharge capacity of 500 mAh· g^{-1}, with a first cycle columbic efficiency of 65%. BC_4N shows excellent cycling stability with almost constant specific capacity higher than 500 mAh· g^{-1}. The charging/discharging efficiency of subsequent n cycles, $\eta' = C_{extrn}/C_{insn} \times 100\%$ reaches ~99% from the 10th cycle.

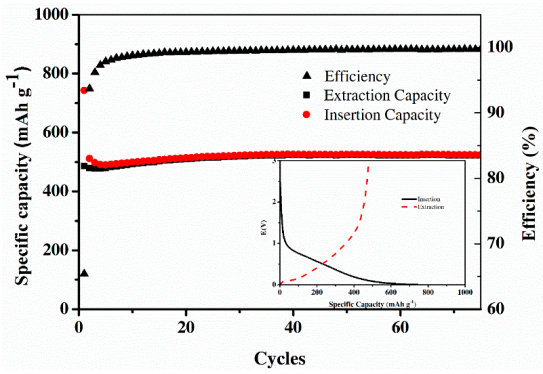

Figure 6. Cycling of BC_4N electrode for 75 cycles at 100 mA· g^{-1}. Inset shows the first cycle charging/discharging profile.

With respect to carbon-poor BC_2N, carbon-rich BC_4N electrodes showed a significantly larger reversible capacity. The columbic efficiency of 73% for the initial slow rate lithiation/delithiation cycle is registered for BC_4N composition. The enhanced electrochemical lithium storage properties registered for BC_4N with respect to BC_2N are attributed to the increased amount of carbon content in the BC_4N material, which is 65 wt % with respect to 45 wt % present within the BC_2N structure. It has been already reported in previous studies that increasing carbon content in BCN-based anodes increases the electrochemical lithium storage capacities [40]. Raman investigation also reveals significant changes in the structure of the materials, namely, a much higher lateral cluster size, La = 10.3 nm, found for the BC_4N material. The La value for amorphous BC_2N amounts to 7.43 nm, respectively. It signifies that more ordered carbon (higher La) might also enhance lithium storage performance. However, we assume that a decreased carbon content, which serves as the major active phase for reversible Li insertion in polymer-derived SiCN and SiOC ceramics [14,15,23,26], is the main reason for diminished electrochemical performance of BC_2N.

The complex nanostructure of BCN materials makes it difficult to identify the Li storage mechanism inside this ceramic matrix. The presence of boron and nitrogen atoms having different electronic configuration in a largely distributed free carbon network may help in attracting excess electrons and make way for more lithium storage. Boron can also act as an electron acceptor, facilitating fast lithium ion diffusion through the doped carbon matrix. A clear mechanism for lithium insertion in the case of BCN-based anodes has not been reported in the literature yet. Kawaguchi *et al.* [45] stated that the amorphous nature is the main reason for poor cycling stability and high irreversible capacity reported for BCN ceramics [40]. Higher crystallinity of BC_6N made the potentials of lithium insertion/extraction to this material lower, and insertion/extraction *E* (V) *vs.* time transients flatter than those of lower crystallinity, which is in good analogy to the relation between graphite and non-graphitic carbon [55]. It is stated that rapid intercalation of lithium ions into crystalline BCN ceramic results in the formation of the first stage intercalation compound Li_xBC_6N. This, in turn, suggests a strong interaction between the intercalate Li and the host material BC_6N. The first stage compound of Li_xBC_6N prepared by the electrochemical method had the d-spacing of 0.355 nm, which is smaller than that of the first stage GIC LiC_6 (0.370 nm). Nevertheless, the capacities of first extraction do not exceed 300 mAh$\cdot$ g^{-1}, and fading is found for subsequent cycles. Lei *et al.* [39] synthesized BCN nanosheets and registered a very good rate capability and reasonable stability; however, the low rate capacity does not exceed 400 mAh$\cdot$ g^{-1}.

Within this study, we investigated the BCN ceramics of amorphous nature, which recover a stable capacity of 500 mAh$\cdot$ g^{-1}. Although BC_4N contains less carbon than that of crystalline BC_6N [45], it demonstrated significantly enhanced electrochemical performance. The capacity stabilizes after several cycles when cycled with increasing currents, while, with a constant current of C/5, extremely stable behavior over 70 cycles and high capacity of ~500 mAh$\cdot$ g^{-1} was registered. We can explain these excellent electrochemical properties with respect to crystalline BC_6N by an analogous comparison with graphite and disordered carbon. Whereas graphite with its common staging intercalation behavior presents low voltage plateaus but low capacity, disordered carbons often demonstrate hysteresis in their potential *vs.* capacity curves but a much higher capacity and rate capability [1]. In a similar way, the capacity of crystalline BCN ceramics is limited by the ordered graphite-like structure. The compounds investigated within this study can store much more lithium due to their disordered nature.

3. Materials and Methods

Amorphous BC_2N and BC_4N were synthesized in an argon atmosphere via thermal conversion of piperazine–borane and pyridine–borane, respectively, up to 1050 °C and 2 h hold time (100 °C/h heating rate) [46,56,57]. The reaction proceeded via the formation of a highly cross-linked and hence insoluble and infusible polymeric intermediate; hence, these are also called polymer-derived ceramics. The carbon, nitrogen, and oxygen content in the final BCN ceramics was determined by hot gas extraction/combustion analysis using LECO C-200 and LECO TC-436, with the accuracies

of 5 ppm and 1% of the measured amount, respectively. Angle-dispersive X-ray powder diffraction data were collected by using STOE STADI P diffractometer with Mo-Kα1 (λ = 0.70931 Å) radiation with a position-sensitive detector having a 6° aperture. Raman spectra were taken with a confocal micro-Raman spectrometer Horiba HR 800 (Horiba, Japan) using an Ar-Ion (Blue) laser with a wavelength of 488 nm. Transmission electron microscopy (TEM) and energy-dispersive X-ray spectroscopy (EDX) studies were carried out using a Jeol JEM 2100F field emission transmission electron microscope equipped with an Oxford X-max80 EDX detector.

Electrochemical characterization was carried out using a Swagelok® type cell assembly, with lithium metal as the counter/reference electrode (99.9% purity, 0.75 mm thick, Alfa Aesar, Karlsruhe, Germany) and 1 M $LiPF_6$ in ethylene carbonate and diethyl carbonate mixture of volume ratio 1:1 (LP 30, Merck KGaA, Darmstadt, Germany) as the electrolyte. A QMA Whatman™ quartz microfiber filter (GE Healthcare Life Sciences, Buckinghamshire, UK) separator was used between the electrodes. The BCN samples were air sensitive, and the electrode coating was made inside an argon filled glove box (MBraun). The working electrode was made of 85 wt % of BCN + 10 wt % polyvinylidenefluoride (PVDF, Solvay, Sembach, Germany) + 5 wt % Carbon Black Super P® (Timcal Ltd., Bodio, Switzerland) black. *N*-methyl pyrolidone (NMP, BASF, Ludwigshafen, Germany) was used as solvent, and the slurry was then coated on a copper foil (10 µm, Copper SE-Cu58, Carl Schlenk Metallfolien AG, Roth, Germany) using a hand blade. The coating was allowed to dry overnight inside the glove box, and electrodes with a diameter of 6 mm were cut from the coating. The obtained electrodes were weighed and dried under vacuum at 80 °C for 24 h using a Buchi oven, prior to cell assembly. The average electrode loading was ~2 mg$\cdot$ cm^{-2}. The electrodes were then transferred again into an argon filled glove box (MBraun) for cell assembly.

The assembled cells were subjected to galvanostatic charging/discharging studies within a potential window of 0.005–3 V with different current densities using a VMP multipotentiostat (BioLogic Science instruments). The current densities were increased step by step after a specified number of cycles and from a faster charging rate of C-rate to 2 C rate. The Galvanostatic Cycling with Potential Limitation (GCPL) cycling rates used were C/20 × 2 + C/10 × 5 + C/5 × 5 + C/2 × 20 + C × 50 + 2 C × 50 + C/20 × 2. Each discharging was performed using the corresponding charging rate (C = D = 360 mA$\cdot$ g^{-1}). The cells were subjected to the initial charging rate after the complete cycling to check the reproducibility of the system.

4. Conclusions

Amorphous BC_2N and BC_4N ceramics were synthesized and investigated towards lithium storage properties. It was found that the BC_4N composition delivers reversible Li storage capacity as high as 735 mAh$\cdot$ g^{-1} at a slow rate of C/20 and has a stable capacity of ~500 mAh$\cdot$ g^{-1} at a charging/discharging rate of 100 mA$\cdot$ g^{-1} during extended cycling. Low carbon BC_2N composition has lower specific capacities, but presents stable behavior over extended cycling. Both the B–C–N compounds are able to recover their initial capacities after cycling the cells for 135 cycles, indicating stability of the BCN-microstructure towards multiple lithiation/delithiation. Interesting electrochemical properties of this material are generally explained in connection with their amorphous nature and with the presence of a high amount of disordered and *in situ*-formed carbon, along with boron and nitrogen heteroatoms distributed in the structural network.

Acknowledgments: Authors acknowledge the financial support from the German Research Foundation (DFG) within SPP 1473/JP8, SPP1236 programs, and the German federal state of Hessen through its excellence program LOEWE "RESPONSE". VSP acknowledge the financial support from the EU through the MC ITN FUNEA, CT-264873. We thank Felix Roth for the help in fitting Raman spectra. The TEM employed for this work was partially funded by the German Research Foundation (DFG/INST163/2951).

Author Contributions: The authors' contribution to the preparation of the manuscript is as follows: Shrikant Bhat: synthesis and characterization of BC_2N and BC_4N ceramics, discussion of the results, and writing of the manuscript; Pradeep Vallachira Warriam Sasikumar: electrochemical characterization, discussion of the results, and writing of the manuscript; Leopoldo Molina-Luna: recording and discussing TEM/SAED; Magdalena

Graczyk-Zajac: discussion and interpretation of the results and writing and proofreading of the manuscript, Hans-Joachim Kleebe: discussion of the results and proofreading of the manuscript, Ralf Riedel: discussion of the results and proofreading of the manuscript.

Conflicts of Interest: The authors declare no conflict of interest.

References

1. Winter, M.; Besenhard, J.O.; Spahr, M.E.; Novak, P. Insertion electrode materials for rechargeable lithium batteries. *Adv. Mater.* **1998**, *10*, 725–763. [CrossRef]
2. Bruce, P.G.; Scrosati, B.; Tarascon, J.M. Nanomaterials for rechargeable lithium batteries. *Angew. Chem.* **2008**, *47*, 2930–2946. [CrossRef] [PubMed]
3. Tarascon, J.-M.; Armand, M. Issues and challenges facing rechargeable lithium batteries. *Nature* **2001**, *414*, 359–367. [CrossRef] [PubMed]
4. Sivakkumar, S.R.; Nerkar, J.Y.; Pandolfo, A.G. Rate capability of graphite materials as negative electrodes in lithium-ion capacitors. *Electrochim. Acta* **2010**, *55*, 3330–3335. [CrossRef]
5. Dahn, J.R.; Zheng, T.; Liu, Y.H.; Xue, J.S. Mechanisms for lithium insertion in carbonaceous materials. *Science* **1995**, *270*, 590–593. [CrossRef]
6. Zhang, W.-J. Lithium insertion/extraction mechanism in alloy anodes for lithium-ion batteries. *J. Power Sources* **2011**, *196*, 877–885. [CrossRef]
7. Zhang, W.-J. A review of the electrochemical performance of alloy anodes for lithium-ion batteries. *J. Power Sources* **2011**, *196*, 13–24. [CrossRef]
8. Shukla, A.K.; Kumar, T.P. Materials for next-generation lithium batteries. *Curr. Sci.* **2008**, *94*, 314–331.
9. Park, C.M.; Kim, J.H.; Kim, H.; Sohn, H.J. Li-alloy based anode materials for Li secondary batteries. *Chem. Soc. Rev.* **2010**, *39*, 3115–3141. [CrossRef] [PubMed]
10. Liu, N.; Shen, J.; Liu, D. A Fe_2O_3 nanoparticle/carbon aerogel composite for use as an anode material for lithium ion batteries. *Electrochim. Acta* **2013**, *97*, 271–277. [CrossRef]
11. Rahman, M.M.; Glushenkov, A.M.; Ramireddy, T.; Tao, T.; Chen, Y. Enhanced lithium storage in Fe_2O_3-SnO_2-C nanocomposite anode with a breathable structure. *Nanoscale* **2013**, *5*, 4910–4916. [CrossRef] [PubMed]
12. Wu, X.L.; Guo, Y.G.; Wan, L.J.; Hu, C.W. α-Fe_2O_3 nanostructures: Inorganic salt-controlled synthesis and their electrochemical performance toward lithium storage. *J. Phys. Chem. C* **2008**, *112*, 16824–16829. [CrossRef]
13. Dibandjo, P.; Graczyk-Zajac, M.; Riedel, R.; Pradeep, V.S.; Soraru, G.D. Lithium insertion into dense and porous carbon-rich polymer-derived SiOC ceramics. *J. Eur. Ceram. Soc.* **2012**, *32*, 2495–2503. [CrossRef]
14. Fukui, H.; Ohsuka, H.; Hino, T.; Kanamura, K. Preparation of microporous Si-O-C composite material and its lithium storage capability. *Chem. Lett.* **2009**, *38*, 86–87. [CrossRef]
15. Fukui, H.; Ohsuka, H.; Hino, T.; Kanamura, K. A Si-O-C composite anode: High capability and proposed mechanism of lithium storage associated with microstructural characteristics. *ACS Appl. Mater. Interfaces* **2010**, *2*, 998–1008. [CrossRef] [PubMed]
16. Graczyk-Zajac, M.; Toma, L.; Fasel, C.; Riedel, R. Carbon-rich SiOC anodes for lithium-ion batteries: Part I. Influence of material UV-pre-treatment on high power properties. *Solid State Ion.* **2012**, *225*, 522–526. [CrossRef]
17. Kaspar, J.; Graczyk-Zajac, M.; Riedel, R. Lithium insertion into carbon-rich SiOC ceramics: Influence of pyrolysis temperature on electrochemical properties. *J. Power Sources* **2013**, *244*, 450–455. [CrossRef]
18. Pradeep, V.S.; Graczyk-Zajac, M.; Riedel, R.; Soraru, G.D. New insights in to the lithium storage mechanism in polymer derived SiOC anode materials. *Electrochim. Acta* **2014**, *119*, 78–85. [CrossRef]
19. Pradeep, V.S.; Graczyk-Zajac, M.; Wilamowska, M.; Riedel, R.; Soraru, G.D. Influence of pyrolysis atmosphere on the lithium storage properties of carbon-rich polymer derived SiOC ceramic anodes. *Solid State Ion.* **2014**, *262*, 22–24. [CrossRef]
20. Shen, J.; Raj, R. Silicon-oxycarbide based thin film anodes for lithium ion batteries. *J. Power Sources* **2011**, *196*, 5945–5950. [CrossRef]
21. Wilamowska, M.; Pradeep, V.S.; Graczyk-Zajac, M.; Riedel, R.; Sorarù, G.D. Tailoring of SiOC composition as a way to better performing anodes for li-ion batteries. *Solid State Ion.* **2014**, *260*, 94–100. [CrossRef]
22. Graczyk-Zajac, M.; Wimmer, M.; Neumann, C.; Riedel, R. Lithium intercalation into SiCN/disordered carbon composite. Part 1: Influence of initial carbon porosity on cycling performance/capacity. *J. Solid State Electrochem.* **2015**, *19*, 2763–2769. [CrossRef]

23. Baek, S.-H.; Reinold, L.M.; Graczyk-Zajac, M.; Riedel, R.; Hammerath, F.; Buchner, B.; Grafe, H.-J. Lithium dynamics in carbon-rich polymer-derived SiCN ceramics probed by nuclear magnetic resonance. *J. Power Sources* **2014**, *253*, 342–348. [CrossRef]
24. Liu, G.; Kaspar, J.; Reinold, L.M.; Graczyk-Zajac, M.; Riedel, R. Electrochemical performance of DVB-modified SiOC and SiCN polymer-derived negative electrodes for lithium-ion batteries. *Electrochim. Acta* **2013**, *106*, 101–108. [CrossRef]
25. Reinold, L.M.; Graczyk-Zajac, M.; Gao, Y.; Mera, G.; Riedel, R. Carbon-rich SiCN ceramics as high capacity/high stability anode material for lithium-ion batteries. *J. Power Sources* **2013**, *236*, 224–229. [CrossRef]
26. Wilamowska, M.; Graczyk-Zajac, M.; Riedel, R. Composite materials based on polymer-derived SiCN ceramic and disordered hard carbons as anodes for lithium-ion batteries. *J. Power Sources* **2013**, *244*, 80–86. [CrossRef]
27. Graczyk-Zajac, M.; Fasel, C.; Riedel, R. Polymer-derived-SiCN ceramic/graphite composite as anode material with enhanced rate capability for lithium ion batteries. *J. Power Sources* **2011**, *196*, 6412–6418. [CrossRef]
28. Reinold, L.M.; Yamada, Y.; Graczyk-Zajac, M.; Munakata, H.; Kanamura, K.; Riedel, R. The influence of the pyrolysis temperature on the electrochemical behavior of carbon-rich SiCN polymer-derived ceramics as anode materials in lithium-ion batteries. *J. Power Sources* **2015**, *282*, 409–415. [CrossRef]
29. Graczyk-Zajac, M.; Wimmer, M.; Neumann, C.; Riedel, R. Lithium intercalation into SiCN/disordered carbon composite. Part 1: Influence of initial carbon porosity on cycling performance/capacity. *J. Solid State Electrochem.* **2015**, *19*, 2763–2769. [CrossRef]
30. Bhandavat, R.; Singh, G. Improved electrochemical capacity of precursor-derived Si(B)CN-carbon nanotube composite as Li-ion battery anode. *ACS Appl. Mater. Interfaces* **2012**, *4*, 5092–5097. [CrossRef] [PubMed]
31. David, L.; Bhandavat, R.; Barrera, U.; Singh, G. Polymer-derived ceramic functionalized MoS_2 composite paper as a stable lithium-ion battery electrode. *Sci. Rep.* **2015**, *5*, 1–7. [CrossRef]
32. David, L.; Bernard, S.; Gervais, C.; Miele, P.; Singh, G. Facile synthesis and high rate capability of silicon carbonitride/boron nitride composite with a sheet-like morphology. *J. Phys. Chem. C* **2015**, *119*, 2783–2791. [CrossRef]
33. Bhandavat, R.; Singh, G. Stable and efficient Li-ion battery anodes prepared from polymer-derived silicon oxycarbide carbon nanotube shell/core composites. *J. Phys. Chem. C* **2013**, *117*, 11899–11905. [CrossRef]
34. Kaspar, J.; Graczyk-Zajac, M.; Lauterbach, S.; Kleebe, H.-J.; Riedel, R. Silicon oxycarbide/nano-silicon composite anodes for Li-ion batteries: Considerable influence of nano-crystalline *vs.* nano-amorphous silicon embedment on the electrochemical properties. *J. Power Sources* **2014**, *269*, 164–172. [CrossRef]
35. Choi, S.; Jung, D.S.; Choi, J.W. Scalable fracture-free SiOC glass coating for robust silicon nanoparticle anodes in lithium secondary batteries. *Nano Lett.* **2014**, *14*, 7120–7125. [CrossRef] [PubMed]
36. Graczyk-Zajac, M.; Reinold, L.M.; Kaspar, J.; Sasikumar, P.V.W.; Soraru, G.-D.; Riedel, R. New insights into understanding irreversible and reversible lithium storage within SiOC and SiCN ceramics. *Nanomaterials* **2015**, *5*, 233–245. [CrossRef]
37. Kaspar, J.; Graczyk-Zajac, M.; Riedel, R. Determination of the chemical diffusion coefficient of Li-ions in carbon-rich silicon oxycarbide anodes by electro-analytical methods. *Electrochim. Acta* **2014**, *115*, 665–670. [CrossRef]
38. Bhandavat, R.; Pei, Z.; Singh, G. Polymer-derived ceramics as anode material for rechargeable Li-ion batteries: A review. *Nanomater. Energy* **2012**, *1*, 324–337. [CrossRef]
39. Lei, W.W.; Qin, S.; Liu, D.; Portehault, D.; Liu, Z.W.; Chen, Y. Large scale boron carbon nitride nanosheets with enhanced lithium storage capabilities. *Chem. Commun.* **2013**, *49*, 352–354. [CrossRef] [PubMed]
40. Ishikawa, M.; Nakamura, T.; Morita, M.; Matsuda, Y.; Tsujioka, S.-I.; Kawashima, T. Boron-carbon-nitrogen compounds as negative electrode matrices for rechargeable lithium battery systems. *J. Power Sources* **1995**, *55*, 127–130. [CrossRef]
41. Machnikowski, J.; Frackowiak, E.; Kierzek, K.; Waszak, D.; Benoit, R.; Béguin, F. Lithium insertion into boron containing carbons prepared by co-pyrolysis of coal-tar pitch and borane-pyridine complex. *J. Phys. Chem. Solids* **2004**, *65*, 153–158. [CrossRef]
42. Rao, C.N.R.; Gopalakrishnan, K.; Govindaraj, A. Synthesis, properties and applications of graphene doped with boron, nitrogen and other elements. *Nano Today* **2014**, *9*, 324–343. [CrossRef]
43. Yin, G.; Gao, Y.; Shi, P.; Cheng, X.; Aramata, A. The effect of boron doping on lithium intercalation performance of boron-doped carbon materials. *Mater. Chem. Phys.* **2003**, *80*, 94–101. [CrossRef]

44. Wu, Z.-S.; Ren, W.; Xu, L.; Li, F.; Cheng, H.-M. Doped graphene sheets as anode materials with superhigh rate and large capacity for lithium ion batteries. *ACS Nano* **2011**, *5*, 5463–5471. [CrossRef] [PubMed]
45. Kawaguchi, M.; Imai, Y.; Kadowaki, N. Intercalation chemistry of graphite-like layered material BC_6N for anode of li ion battery. *J. Phys. Chem. Solids* **2006**, *67*, 1084–1090. [CrossRef]
46. Bill, J.; Riedel, R.; Passing, G. Amin-borane als precursoren für borcarbidnitrid. *Z. Anorg. Allg. Chem.* **1992**, *610*, 83–90. [CrossRef]
47. Hubacek, M.; Sato, T. Preparation and properties of a compound in the B-C-N system. *J. Solid State Chem.* **1995**, *114*, 258–264. [CrossRef]
48. Shrikant, B.; Stefan, L.; Dmytro, D.; Christian, L.; Lkhamsuren, B.; Marcus, S.; Hans-Joachim, K.; Edwin, K.; Björn, W.; Ralf, R. High-pressure high-temperature behavior of polymer derived amorphous B-C-N. *J. Phys. Conf. Ser.* **2014**, *500*, 182004.
49. Watanabe, M.O.; Itoh, S.; Mizushima, K.; Sasaki, T. Bonding characterization of BC_2N thin films. *Appl. Phys. Lett.* **1996**, *68*, 2962–2964. [CrossRef]
50. Watanabe, M.O.; Sasaki, T.; Itoh, S.; Mizushima, K. Structural and electrical characterization of BC_2N thin films. *Thin Solid Films* **1996**, *281–282*, 334–336. [CrossRef]
51. Marton, D.; Boyd, K.J.; Al-Bayati, A.H.; Todorov, S.S.; Rabalais, J.W. Carbon nitride deposited using energetic species: A two-phase system. *Phys. Rev. Lett.* **1994**, *73*, 118–121. [CrossRef] [PubMed]
52. Matizamhuka, W.R.; Sigalas, I.; Herrmann, M.; Dubronvinsky, L.; Dubrovinskaia, N.; Miyajima, N.; Mera, G.; Riedel, R. Characterization of the materials synthesized by high pressure-high temperature treatment of a polymer derived t-BC_2N ceramic. *Materials* **2011**, *4*, 2061. [CrossRef]
53. Cancado, L.G.; Takai, K.; Enoki, T.; Endo, M.; Kim, Y.A.; Mizusaki, H.; Jorio, A.; Coelho, L.N.; Magalhaes-Paniago, R.; Pimenta, M.A. General equation for the determination of the crystallite size la of nanographite by Raman spectroscopy. *Appl. Phys. Lett.* **2006**, *88*, 163106–163106. [CrossRef]
54. Sadezky, A.; Muckenhuber, H.; Grothe, H.; Niessner, R.; Poeschl, U. Raman microspectroscopy of soot and related carbonaceous materials: Spectral analysis and structural information. *Carbon* **2005**, *43*, 1731–1742. [CrossRef]
55. Kanamura, K.; Shiraishi, S.; Takezawa, H.; Takehara, Z.-I. XPS analysis of the surface of a carbon electrode intercalated by lithium ions. *Chem. Mater.* **1997**, *9*, 1797–1804. [CrossRef]
56. Riedel, R.; Bill, J.; Passing, G. A novel carbon material derived from pyridine-borane. *Adv. Mater.* **1991**, *3*, 551–552. [CrossRef]
57. Riedel, R. Materials harder than diamond? *Adv. Mater.* **1992**, *4*, 759–761. [CrossRef]

© 2016 by the authors; licensee MDPI, Basel, Switzerland. This article is an open access article distributed under the terms and conditions of the Creative Commons by Attribution (CC-BY) license (http://creativecommons.org/licenses/by/4.0/).